3.3 Wave-particle Physics, Heating, and Current Drive

The ST plasma parameters provide a unique laboratory for studying wave-plasma interactions in the high β, high dielectric constant regime. On NSTX, the new heating and current drive scenarios utilizing HHFW and EBW are being explored. Initial studies have indicated the potential for strong electron damping and current drive, as well as the possibility of strong coupling of externally-launched X (or O) modes to electron Bernstein waves inside the plasma and subsequent localized current drive. These techniques show promise for application to a variety of fusion concepts, including compact stellarators, Reverse Field Pinches, spheromaks and burning plasma devices.

3.3.1 High Harmonic Fast Wave Goals

The IPPA-FESAC five-year research objective, "Preliminary Assessment of ST Performance", and the 10-year research objective, "Assessment of The Attractiveness of The ST Concept for Pulse Lengths Long Compared to The Current Diffusion Time", require tools to heat and drive current supplemental to the ohmic systems. One such tool is RF wave heating and current drive utilizing the fast magnetosonic wave at high harmonics of the ion-cyclotron frequency. Up through the first five-year assessment point of the plan, to be reached in 2006, a comprehensive evaluation of HHFW as a tool for enhancing ST performance, heating current drive and startup, will be performed. It will be applied to help meet the goals (i.e., moderate beta and bootstrap fraction) of fully non-inductive operations for plasma parameters relevant to a component test facility, and will also be used in discharges demonstrating solenoid-free plasma current ramp-up to high beta operations. Afterwards, HHFW will be utilized in conjunction with other techniques to further reduce volt-second consumption and to assist long-pulse operations for the highest beta plasmas.

3.3.2 HHFW Physics

High harmonic fast waves are expected to primarily interact with electrons, making this type of heating a strong candidate for driving current in ST plasmas [1]. Wave accessibility in the naturally occurring high

 plasmas of an ST precludes the use of conventional ECH or lower-hybrid heating or current drive except for the possibility of plasma startup in low-beta plasmas. Current-drive efficiencies with HHFW waves are expected to be comparable to other fast wave and ECH techniques since they drive the same class of electrons near the thermal velocity. However, in spite of the large ratio of ω/ω_{ci}, 9-13, on NSTX at large values of β_i some power will damp on thermal ions. In addition, due to the large value of $k_\perp \rho_i$ for NBI ions, they can absorb appreciable power [2]. These competing absorption paths, as well as toroidal electron trapping effects may reduce the current drive efficiency in some parameter regimes. An alternate high-frequency RF technique that utilizes mode converted EBW will be explored as well and will be discussed in Sections 3.3.7-3.3.12.

3.3.3 The HHFW System

The HHFW on NSTX utilizes much of the ICRF system from TFTR [3]. The frequency employed, 30 MHz, is identical to that used on TFTR. Due to the much reduced toroidal magnetic field of NSTX, compared to TFTR, this corresponds to moving from $\omega=2\omega_T$ to $\omega=10\omega_D$. Transmitters were left in place and the transmission line from the transmitters to the tuning network was untouched, and the output of the tuning network was rerouted from the entrance to the TFTR test cell to the NSTX test cell. The antenna and the external power dividing and phasing network were constructed specifically for NSTX.

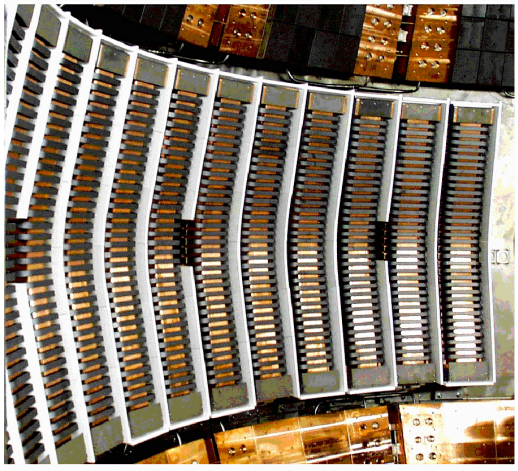

Figure 3.3.1 The twelve-strap HHFW antenna array.

The antenna consists of 12 independent antenna modules. Each module contains a radiating element grounded at the bottom to the enclosure box and fed at the other end through an RF feedthrough and spool piece. The radiating element is separated from the plasma by a 50% transparent single-layer Faraday screen composed of individual u-shaped elements. Exterior to the vacuum vessel is a system of transmission lines and tuning elements that divide the power from the six transmitters into twelve feeds, cancel the mutual coupling between adjacent antenna

elements, and allow for the monitoring of antenna voltage, current and phase.

Operation goals of the system include 6 MW of injected power for pulse lengths much longer than a current diffusion time, and potentially as long as 5 s pulses, with real time phase control of the antenna spectrum, and programmed amplitude modulation. In the design phase it was estimated that antenna voltages of ~ 20 kV would be required to support this level of operation. Vacuum conditioning of the antennas to the 25-30 kV level is routinely obtained. Pulse duration during plasma operations has been limited to < 1 s by volt-second limitations. 6 MW of power has been achieved for short pulses, but long pulse power has been limited by arcing in the vacuum region. The reliable long pulse limit has gone from 3.5–4 MW during the 2001 campaign to ~ 2.5 MW during the 2002 campaign. The peak antenna voltage limit for reliable operation was found to be ~ 12kV. During the 2002 outage examination of the antennas by dismantling them uncovered a weak point in the spool-piece/feedthrough area where arcing along the magnetic field was observed. As a result, modifications have been made to increase the spacing and to reduce the electric field stress for a given RF power. These modifications, which were tested in the 2003 operations period, increased the voltage breakdown limit by ~ 40%, as expected..

3.3.4 Status of HHFW Research

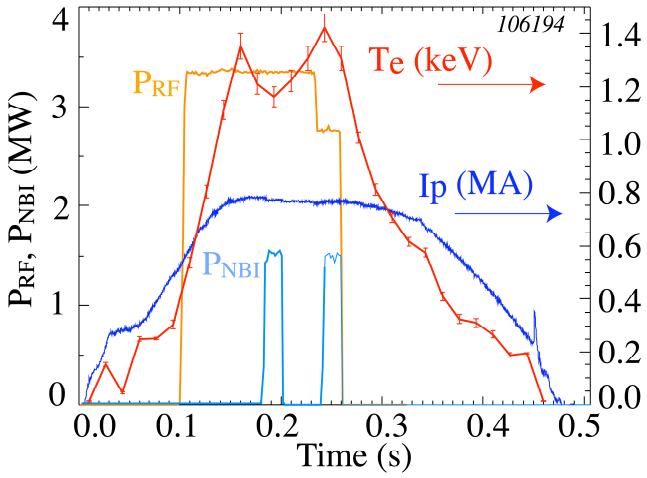

Figure 3.3.2 Electron temperature evolution with HHFW heating.

Experiments on NSTX have confirmed the strong electron damping expected by theory[4]. In the relatively low □ (□ 15%) plasmas investigated so far, no evidence of thermal ion heating has been found. Figure 3.3.2 illustrates the basic heating results obtained on NSTX. The central electron temperature increases strongly with the application of HHFW power. The ion temperature, measured with a short NBI pulse near the end of the RF pulse using charge exchange recombination

spectroscopy, is half the electron temperature. The strong absorption of HHFW waves on electrons allows heating even at the low target temperature of 300 eV. Global energy confinement is found to be in agreement with predictions from conventional scaling. Heating of thermal ions is expected to become appreciable when the ion temperature approaches 2 keV.

Improved confinement discharges have been observed with central electron temperatures reaching 4 keV, (Figure 3.3.3). The confinement improvement is observed over the central half radius with as much as an order of magnitude improvement on-axis. These discharges exhibit a continuous improvement in time, eventually terminating in a crash similar to those observed with PEP modes in conventional tokamaks.

Preliminary experiments on current drive have been performed. In the absence of an internal current profile diagnostic, such as MSE, the only indicator of current drive is the external response of the magnetic diagnostics. To differentiate between direct RF current drive and bootstrap current, these experiments were conducted at low values of β_e and in L-mode. Since NSTX operates in a mode with feedback holding the plasma current constant an internally driven current induces an immediate response in the external power supplies that shows up as a reduced loop voltage required to sustain the same total current. The absolute level of loop voltage required for a given current is a sensitive function of the plasma resistivity, which depends on the electron temperature, density and the plasma Z_{eff}. Discharges with the RF antenna phased to launch directed waves co- and ctr- to the plasma current were carefully matched in density, temperature and Z_{eff} by adjusting the power level and gas fueling rate. The amount of driven current can then be estimated from the formula:

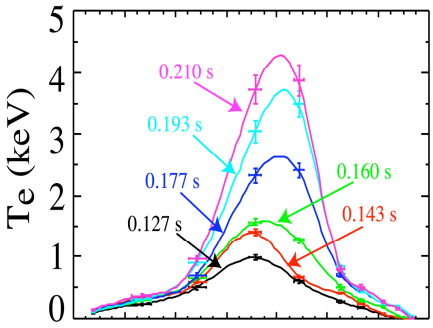

Figure 3.3.3 Temperature profile evolution of an improved confinement HHFW discharge.

$$I_P = (V - 0.5 * I_P * dL_i/dt)/R_P + I_{BS} + I_{CD} \qquad (3.3.1)$$

For these conditions, the loop voltage difference of ~ 0.23 V (Fig. 3.3.4) between co- and ctr- corresponds to ~110 kA of driven current for the co- case. Predictions from the TORIC [5] and CURRAY [6] RF wave deposition and CD codes are in rough agreement with this estimate, yielding 96 and 160 kA respectively. Evidence for current drive has been observed with directed wave spectra between 3 and 7 m^{-1}.

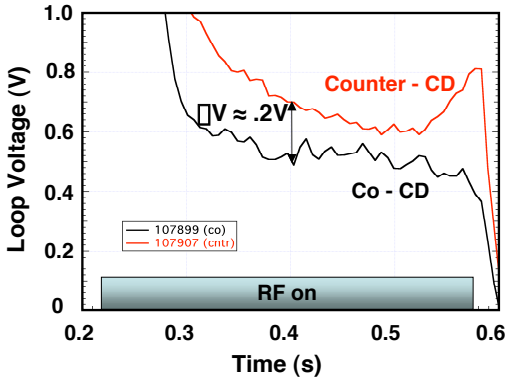

Figure 3.3.4 Loop voltage evolution for co- and ctr- current drive phasing.

In order to demonstrate an attractive fully non-inductive scenario, a large fraction of the current should be driven by the bootstrap current. This is most readily achieved in H-mode discharges with their large values of stored energy and their broad pressure profiles. In Fig. 3.3.5, an H-mode discharge with $\beta_p \sim 1$ and $I_{bs}/I_p \geq 0.4$ is sustained with HHFW heating alone. The discharge has reached transport equilibrium in an elming H-mode but the current profile continues to evolve with q(0) rising and l_i falling to the end of the RF pulse. The H-mode phase terminates with the removal of RF power, which was programmed to go off at the time of TF ramp down. This discharge is an attractive target for long pulse sustainment by phasing the RF for current drive instead of heating.

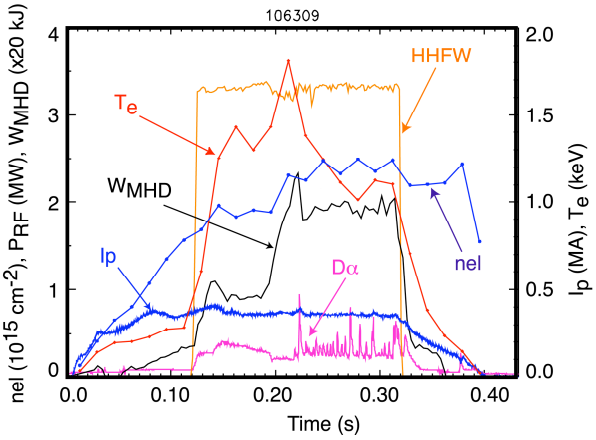

Figure 3.3.5 H-mode discharge with HHFW alone.

The efficiency of RF current drive can be adversely affected by damping of the HHFW power into thermal ions or energetic NBI ions. While heating of the thermal ions has yet to be observed, acceleration of NBI ions to energies above the injection energy has been seen in the presence of HHFW heating in the escaping fast neutral energy spectrum, measured with a charge exchange analyzer. A tail above the 80 keV injection energy is observed extending in some cases to 140 keV (Fig. 3.3.6). The distribution relaxes to its no RF level after the HHFW is turned off (blue and black curves), consistent with classical slowing down upon removal of

the RF power. In addition, enhanced neutron production is measured when the tail is present, confirming its existence in the plasma core. Behavior of the tail as parameters are varied has been investigated to ascertain the seriousness of the power loss. Increasing the electron □ is seen to reduce the tail as expected from theory. In addition, no increase in the tail is observed as the wave $k_{||}$ is reduced in contradiction to theoretical predictions. Both of these results, although preliminary, are positive results for driving significant currents in the high beta long pulse target discharges. More work is needed to understand these results theoretically. In particular, if the lack of increased fast ion absorption with decreasing $n_{||}$ is also true for thermal ions this may improve current drive efficiencies in plasmas with high thermal ion temperatures.

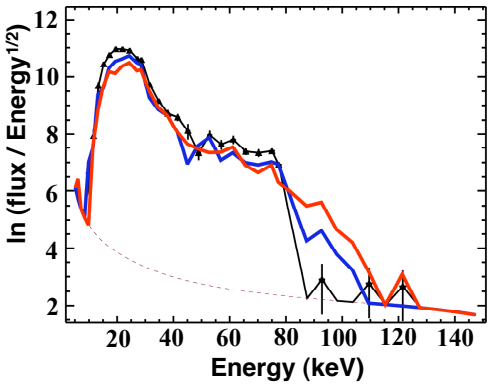

Figure 3.3.6 Escaping fast ion energy distribution as measured by a neutral particle energy analyzer. Full beam energy is 80 keV.

3.3.5 HHFW Theory and Modeling Status

Ono was the first to elucidate the basic theory for high harmonic fast wave (HHFW) heating of high □ plasmas [1]. The fast magnetosonic wave that is used for conventional ICRF heating and current drive is also utilized in the HHFW regime. Consequently, HHFW heating and current drive in an ST share a common foundation, both in physics and technology, with the heating and CD scenarios that have already been extensively studied in conventional and advanced tokamak regimes. Despite this common foundation, there are features unique to the HHFW regime that require significant extensions to the theory and models developed for ICRF heating and current drive in conventional and advanced tokamaks, as discussed in the section on RF Theory and Computation. In this section, some specific applications of theory and modeling to the understanding of NSTX experiment, as well as future development plans, are discussed.

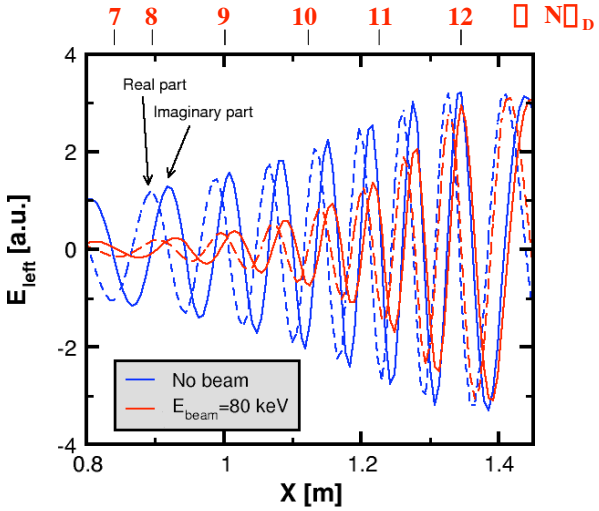

Figure 3.3.7 HHFW electric fields vs. major radius along midplane from METS codes, both with and

Because the launched wave frequency is much higher than the fundamental cyclotron frequency of any ion species in an ST plasma, ion cyclotron damping occurs at high harmonics of the fundamental ion cyclotron frequencies (in NSTX experiments, typically $5 < \omega/\omega_i < 15$). Most computational models developed for conventional tokamaks utilize a finite Larmor radius expansion of the wave fields, an approximation that is strictly valid only for fundamental and second harmonic cyclotron interactions for ions whose gyroradii are small relative to the perpendicular wavelength of the high harmonic fast wave (i.e., valid in the FLR or finite Larmor radius limit). Recently, 1-D [7] and 2-D [8] kinetic wave codes have been developed, which include all cyclotron harmonic interactions and which are valid for ion gyroradii that can be large relative to the HHFW perpendicular wavelengths, but small compared to equilibrium scale lengths. Initial results from these generalized all-orders codes indicate that the wave dynamics in NSTX plasmas with moderate densities and temperatures is dominated by fast-wave physics with electron absorption dominant in this parameter regime, as expected from analytic theory. Mode conversion to short wavelength ion Bernstein waves, which in principle can occur near the various cyclotron harmonics, does not appear to be significant in these plasmas. In Figure 3.3.7, the left-hand component of the fast-wave field obtained from the 1-D all-orders code, METS [7] is shown as a function of distance along the midplane for an NSTX discharge with combined HHFW and NBI heating. No excitation of short wavelength modes is evident near the cyclotron harmonics. Similar results have been obtained with the AORSA-2-D all-orders code [8]. Further numerical studies will be performed to determine if mode conversion is more significant at the higher toroidal fields and hence somewhat lower cyclotron harmonics anticipated in a next-step ST device.

In NSTX plasmas, because of the absence of significant mode conversion and because the ratio of the wavelength to the equilibrium gradient scale lengths is small, ray tracing codes that are based on WKB

approximations may be applicable. Power deposition profiles obtained with ray tracing codes that utilize the full hot plasma dielectric tensor to compute the ion and electron damping compare favorably with those obtained from the all-orders kinetic models for NSTX plasmas with moderate densities and temperatures. In Figure 3.3.8a, excellent quantitative agreement is evident between the power deposition profiles obtained with two ray tracing codes, HPRT9] and CURRAY [6], and in Fig. 3.3.8b with the AORSA 2-D full wave code, and with the TORIC reduced order 2-D full wave code for an NSTX discharge in which the electron damping is predicted to dominate. TORIC [5] is a full-wave code that utilizes the FLR approximation and an extension of the reduced order approximation [10] to solve for the fast-wave fields. Both the ray tracing models and the full-wave reduced-order models usually require far less computational time than the full wave all orders codes, so these simpler models may offer a more practical yet accurate module for integration into a time-dependent transport analysis package, such as TRANSP. The CURRAY ray tracing code and the upgraded TORIC code are both being implemented in TRANSP. This work should be completed in FY03 in order to enable to time-dependent transport analyses of NSTX experiments.

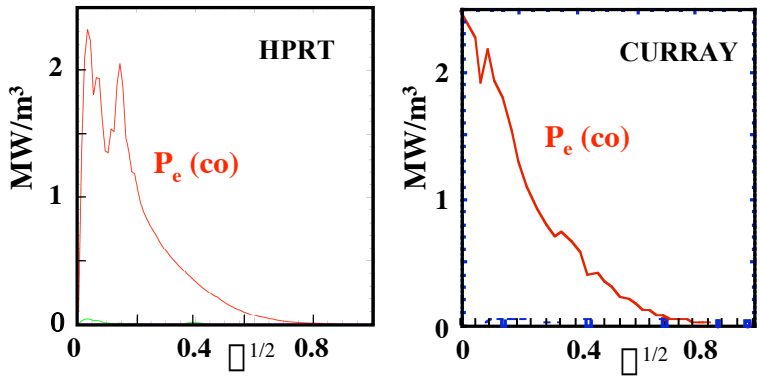

Figure 3.3.8a Comparison of ray tracing analyses for a HHFW current drive discharge.

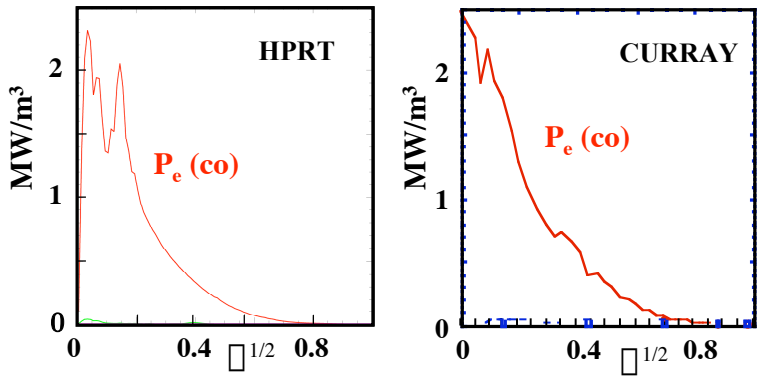

Figure 3.3.8a Comparison of ray tracing analyses for a HHFW current drive discharge.

Damping on energetic ions present in NSTX due to neutral beam injection (NBI) can be significant, since $k_{\perp}\rho_i >>1$ for these ions. In recent experiments on NSTX with combined HHFW heating and neutral beam injection, direct measurement of the fast ion velocity distribution function with the NPA diagnostic indicates that substantial damping of the HHFWs by the energetic ions occurs that is accompanied by a significant distortion of the beam slowing down distribution function [11]. Though the all-orders full-wave models include beam ion absorption when $k_{\perp}\rho_i >>1$, these codes generally assume that the ion velocity distributions are Maxwellian. Recently, as part of the SciDAC initiative, the 1-D METS code has been generalized to compute wave propagation and absorption in plasmas with significant populations of a non-thermal species [12]. Initial results from the generalized 1-D METS code indicate that absorption on isotropic beam distributions may be reasonably approximated by Maxwellian distributions with the same average energy. When anisotropic beam effects are included in these initial 1-D simulations, the predicted fast-ion absorption is reduced by up to a factor of two. This effect is particularly important for beam injection angles below 30°. If verified by experiment, this effect would indicate a corresponding increase in the current-drive efficiency currently estimated by the CURRAY, TORIC and AORSA 2-D codes. However, 2-D effects on wave propagation and absorption are also known to be significant in an ST plasma, as indicated by comparisons of power deposition profiles obtained with 1-D and 2-D models. To address the effects of non-Maxwellian species on 2-D wave propagation and absorption, the 2-D modeling codes will need to be generalized to include non-Maxwellian species in their dielectric tensor operators, as part of the SciDAC initiative.

Since the HHFWs have been observed to modify the beam slowing down distributions, the wave codes must be coupled with a Fokker-Planck code to self-consistently compute the wave propagation and absorption. In the preliminary studies, beam velocity space distribution functions obtained from the TRANSP code will be used to specify the non-Maxwellian species in the wave codes. Eventually, the generalized wave codes must be integrated with a Fokker-Planck code to self-consistently compute the wave propagation, absorption and velocity space modifications. The CQL3D/GENRAY [13] code, which combines ray tracing for wave propagation with a Fokker-Planck package that includes collisions, large-orbit losses and RF quasilinear diffusion in two velocity-space dimensions, will be modified and benchmarked against NSTX data. If full-wave effects are found to be important, then the CQL3D package will be integrated with the generalized 2-D wave codes. It is anticipated that such a combined simulation package will require a significant amount of computation time even on massively parallel

computers and may not be appropriate for use in time-dependent simulations with the TRANSP package.. This code development activity is expected to last through FY05.

Because of the inherently high beta and high dielectric constant in an NSTX plasma, direct electron absorption of the waves via transit time magnetic pumping can be comparable to or greater than direct ion absorption via cyclotron damping, even in plasmas with neutral-beam injection. Unlike the low direct electron damping rates of <15% per pass for fast waves in conventional tokamaks, it is not unusual to expect nearly 100% damping in a single pass through the NSTX plasma. In fact, since the damping is so strong at high β, the wave power can be significantly damped before it reaches the center of the plasma, resulting in off-axis power deposition profiles. When combined with appropriate control of the launched wave spectrum, noninductive control of the off-axis current profile may be possible. However, the current drive efficiencies may be limited by competing absorption by the fast ions and the thermal ions, as well as trapping effects, which can be significant on the low field side of the magnetic axis. Loop voltage measurements in preliminary HHFW current drive experiments (discussed in Section 3.3.4) on NSTX without neutral-beam injection are consistent with the presence of non-inductively driven currents. The experimentally inferred HHFW driven currents are comparable to those estimated with the CURRAY code and with the TORIC code. CURRAY utilizes either the Ehst-Karney parameterization [14] of current-drive efficiency or a full adjoint solution to the Fokker-Planck equation to estimate the driven current profile. At low plasma betas up to about 15%, the parameterization and the adjoint code give similar estimates for the current drive efficiency, according to studies with CURRAY package. Previous studies obtained with an earlier version of the TORIC code coupled to the adjoint code also found that the Ehst-Karney parameterization is adequate for plasma betas up to about 15% [15]. The more recent version of TORIC utilizes the Ehst-Karney parameterization, but development work is underway to couple TORIC with the CQL3D Fokker-Planck package. Further benchmarking of these codes against NSTX will continue, particularly when direct measurements of the driven currents are obtained with the MSE diagnostic. In the meantime, effects of the DC electric field arising from the ohmic current drive system, particle trapping, and electron transport will be incorporated into the full Fokker-Planck models. These theoretical and experimental studies, when combined with the generalized wave codes discussed above, will serve to elucidate the importance of various effects on HHFW heating and current drive in NSTX plasmas.

3.3.6 HHFW Research Plan for 2003-2008

The comprehensive evaluation of HHFW as a tool for use in ST requires experiments and modeling to confirm an understanding of HHFW heating and current drive physics sufficient to predict its performance in future ST experiments. In the case of heating this should include an understanding of: operations in various plasma configurations, the behavior as density is controlled with gas puffing, H-mode behavior with RF, radial localization of heating as a function of plasma parameters and launched spectrum, and improved confinement regimes. For current drive this evaluation should include an understanding of efficiency as a function of plasma parameters and phase, as well as configuration. Competing absorption on thermal and fast ions is a particular concern.

Configuration and density dependence of HHFW coupling

2003–2004:

HHFW heating experiments have mostly been performed in limiter or lower single-null configurations. Double null configurations and various values of inner and outer gap parameters should be explored. For example, preliminary data show an inverse relationship between inner gap and stored energy.
Finally, as density is raised by gas puffing, heating efficiency as measured by the central electron temperature is reduced. This may be due to a broadening of the deposition profile, a reduction in global confinement or damping of the RF power in the plasma periphery. Density control will be studied over a wider range of density owing to improved fueling capability and wall preparation techniques, as discussed in the section on boundary physics. Heating of the thermal ion population will be explored utilizing the new x-ray crystal diagnostic to measure the ion temperatures. H-mode discharges should provide the higher target ion temperatures that theory indicates are required for significant ion absorption.

HHFW with heating phasing as a pressure and current profile modification tool – Heating with HHFW can modify the q profile through electron heating directly, particularly during the current ramp phase, even in the absence of current phasing. For example, higher electron temperatures can increase the plasma conductivity, thereby increasing the current diffusion time, can increase the plasma bootstrap current, and can increase the neutral beam current drive by increasing the fast ion slowing down time.

HHFW heating, coupling with NBI, and profile modification

2003–2004:

*Internal inductance modification through heating early in the discharg*e – Already HHFW heating in the current ramp phase has resulted in voltage second savings, reduced the plasma internal inductance and increased q(0). This work will continue and will benefit from improved plasma control and understanding of gap and configuration dependence of HHFW efficiency.

Effective coupling of HHFW with neutral beam heating – A research focus in 2003 and 2004 will be the assessment of HHFW heating effectiveness in the presence of strong neutral beam heating. The efficiency of HHFW heating as a function of target plasma conditions, including plasma beta and density, will be assessed.

HHFW H-modes – H mode plasmas have been produced by HHFW heating alone and are promising targets for achieving the ultimate NSTX goals. The exact conditions under which H-modes are obtained with RF have received little attention to date. Threshold power as a function of plasma parameters needs to be determined. The conditions for achieving ELM-free or ELMy H-modes will be established, as will the configuration space for achieving the best H-mode/HHFW performance.

2005–2006:

Initial feedback control of HHFW heating – Application of HHFW to high-beta plasma targets should yield off-axis HHFW deposition, potentially enabling broadening of the electron thermal pressure profile. Initial work in feedback of HHFW will begin toward the end of this research period.

2007–2008:

Advanced feedback control of HHFW heating and current drive is described below.

Current drive studies and wave-particle interactions

2003–2005:

Current drive studies at high power – The first current drive studies in 2004 will take advantage of improved high-voltage standoff and higher power levels for longer pulse, enabling more definitive

assessments of current drive via observations of the surface loop voltage to be obtained. These experiments will continue the investigations begun in 2002 exploring higher power, higher temperature plasma and a wider range of wave spectra. In addition, during the latter part of the 2004 campaign it is expected that the MSE diagnostic will be commissioned and be in preliminary operation. Experiments with a fully operational MSE diagnostic are expected in the 2005 time frame. These experiments will explore the radial location of the driven current and the ability to control it. Wave-fast particle interactions studies, which may partly determine the efficiency of HHFW current drive and heating, will use measurements of the escaping fast-ion distribution.

2005–2006:

Parametric dependencies – For current drive, it is important to establish the efficiency as a function of RF power, density, temperature, and antenna phasing. Early in this period, such dependencies will be explored. Present scenarios being examined suggest that NSTX non-inductive sustained operation in 15–20% toroidal beta plasmas relevant to a component test facility will require driven currents of about 100 kA with upwards of 5 MW of HHFW heating in the presence of substantial bootstrap current (see Chapter 4 on Integrated Scenario Development). Achieving higher amounts of driven current at lower input powers will add highly desirable flexibility for these scenarios. The MSE diagnostic will allow an investigation of the radial location of current drive and an exploration of the role of trapping in reducing current-drive efficiency. Trapping is calculated to reduce the driven current in present experiments by as much as a factor of four. It should play a larger role in off-axis current drive but its role may be reduced at high beta by the diamagnetic effect.

2007–2008:

a. Phase feedback on current profile modifications – Phase modification within a discharge has already been demonstrated with the HHFW system. Real-time assessment of changes in the magnetic field pitch angle due to current profile changes will be possible with the MSE laser-induced fluorescence (LIF) system. It is therefore possible to modify the antenna phasing in response to modifications in the current profile in real time. Implementation of this capability will begin in the 2007 time frame.

b. Advanced HHFW heating and current drive feedback control – HHFW will be used in both heating and current drive phasing with full feedback control of the antenna phase. The MSE LIF system will be used

to measure the local current density, local plasma pressure, and radial electric field changes in real time. In conjunction with the NSTX control system and the HHFW real-time power and phasing control capability, this will allow for advanced feedback control of the pressure and current profiles.

Solenoid-free plasma startup

The use of HHFW in these studies is discussed in additional detail in Chapter 4.

2004–2005:

Coupling with Coaxial Helicity Injection – In this time period, the transient application of coaxial helicity injection will be used to initiate a plasma discharge without the use of a solenoid. The plasma control system will be used to maintain position control of the reconnected plasma. Following on studies where the CHI is coupled to ohmic plasmas early in 2004, the next step will be the application of HHFW heating to increase β and develop bootstrap currents, and the application of HHFW with current drive phasing for the direct drive of current.

2006–2007:

Handoff to NBI during current ramp – When the current is driven to a level high enough to enable effective confinement of fast ions, neutral beam injection will be applied to allow bootstrap current and direct neutral beam current drive to carry the plasma current to a high poloidal beta flattop.

2007–2008:

Optimization of flux consumption in high performance plasmas – Techniques for flux savings developed in this research will be applied to the optimization of plasmas with toroidal beta values approaching 40%, in pursuit of the demonstration of advanced, high-performance ST operating scenarios in plasmas with 100% non-inductive current drive..

Technical modifications to the HHFW system

2004–2005:

Possible additional modifications for reliability at high voltages – The antenna voltage limit must be raised to achieve routine 6 MW operation. Recently made modifications increased this limit by the

expected amount of ~ 40% and further improvement should be possible by going to a double-ended configuration from the present single-ended one. This would require significant modification of the antenna (new radiation elements). Even if the present modification works to 6 MW, the further change might be justified by allowing even higher power, which is available from the transmitters, or a reduction in the number of antenna elements yielding more room for diagnostics.

3.3.7 Electron Bernstein Wave (EBW) Research Program Goals

Recent experiments on CDX-U and NSTX have demonstrated that mode conversion of EBWs, emitted by thermal fluctuations in these overdense plasmas, to the X-mode can be controlled by modifying the edge density profile with a local limiter. Based on the success of these passive emission experiments, the NSTX EBW heating (EBWH) and current drive (EBWCD) research program for the period 2003 to 2008 has four major goals. The first goal is to demonstrate efficient coupling of X (or O) mode waves to EBWs for high-input powers (in the megawatt range). The second goal is to control the spatial location where the EBWs damp on electrons and, subsequently, heat them. These first two goals are in support of the IPPA five-year milestone 3.2.1.3 to heat high β over-dense plasmas. The third goal is to test EBW-assisted non-inductive current startup either alone or in combination with HHFW and/or CHI. This goal supports the IPPA five-year milestone 3.2.1.4 to make a preliminary assessment of non-inductive spherical torus (ST) startup. The fourth goal is to test neoclassical tearing mode suppression with EBW heating and/or current drive to help sustain a high β plasma for up to a one-second duration. This goal supports the IPPA five-year milestone 3.2.1.2 to suppress β-limiting MHD modes. In order to accomplish these research goals within the time period covered by the five-year plan, we plan to install about one megawatt of EBW heating capability, which would be operational on NSTX no later than 2006. The plan also includes an upgrade to a 3 MW EBW heating and current drive system during the period 2006 to 2008 to provide off-axis current drive to stabilize plasmas with β ~ 40% during this time. This latter goal supports the IPPA ten-year milestone to assess the attractiveness of ST operation for pulse lengths much longer than the current penetration time scale.

3.3.8 Status of EBW Research and Near-Term Plans

For low-β, large aspect ratio devices, such as conventional tokamaks, current profile control can be provided by ECCD, but for high-β plasmas, like the ST, RFP, and spheromak, the plasma is over-dense ($\omega_{pe}/\omega_{ce} >> 1$), precluding the use of ECCD and ECH. EBWs on the other hand have the potential to heat and drive current in STs, since these waves propagate in over-dense plasma and are strongly absorbed near the electron cyclotron resonances.

The EBW emission, heating and current drive research program has so far been focused on two areas of research; optimization of the mode conversion and coupling between electromagnetic modes and EBWs and the identification and characterization of current drive and heating scenarios for NSTX equilibria through the use of ray tracing and Fokker-Planck deposition codes. Experiments to maximize EBW mode conversion to the X-mode have already demonstrated > 95% EBW to X-mode conversion on CDX-U and up to 50% EBW to X-mode conversion on NSTX. These experiments were conducted to support the development of an EBW emission diagnostic for $T_e(R,t)$ measurements, as well as the proposed NSTX EBW heating and current drive program discussed here. Experiments that aim to demonstrate ≥ 80% EBW to electromagnetic mode conversion via emission measurements with a local limiter are planned for the 2004 NSTX run campaign.

3.3.9 Status of EBW Coupling Theory and Modeling

EBW mode conversion (MC) can occur via two processes. The first process involves conversion of EBWs to the fast X-mode [16-18]. EBWs first convert to the slow X-mode at the upper hybrid resonance (UHR). A cutoff-resonance-cutoff triplet formed by the left hand cutoff of the slow X-mode, the UHR, and the right hand cutoff of the fast X-mode allows the slow X-mode to tunnel through the UHR to the fast X-mode (B-X conversion). This is the conversion process so far investigated on CDX-U and NSTX.

The mode conversion efficiency (C) for $k_{//} = 0$ is given by [18]:

$$C = 4e^{-\pi\eta}\left(1 - e^{-\pi\eta}\right)\cos^2(\pi/2 + \pi) \qquad (3.3.2)$$

where $\cos^2(\pi/2+\delta)$ is a phase factor relating to the phasing of the waves in the mode conversion region and the term preceding this is the maximum mode conversion efficiency. Here δ is a tunneling parameter, which for magnetic scale lengths much greater than the density scale length at the UHR [18], is given by:

$$\delta \approx \left[\omega_{ce} L_n / (c\beta)\right]\left[(1+\beta^2)^{1/2} - 1\right]^{1/2} \qquad (3.3.3)$$

where L_n, the density scalelength, and $\beta = \omega_{pe}/\omega_{ce}$ are evaluated at the UHR layer and c is the velocity of light. From these equations it can be seen that the B-X conversion efficiency is very sensitive to changes in L_n at the UHR layer where the wave frequency, $\omega = \omega_{UHR}$. B-X mode conversion is particularly well suited for ST plasmas since the UHR layer for fundamental EBW conversion lies in the scrape off layer outside the last closed flux surface (LCFS) where L_n can be modified without affecting plasma performance. On CDX-U and NSTX the maximum mode conversion efficiency for fundamental EBWs occurs for $L_n \sim$ 0.3-0.6 cm.

The second mode conversion process requires the coincidence of the X-mode and O-mode cutoffs [19-23] (B-X-O conversion), and has been studied extensively on Wendelstein 7-AS both for heating [24] and as a $T_e(R)$ emission diagnostic [25]. The B-X-O emission leaves the plasma through an angular window at an oblique angle with a transmission function given by [21,23]:

$$T(N_\perp, N_{//}) = \exp\left\{-\pi k_o L_n \sqrt{(Y/2)}\left[2(1+Y)(N_{//,opt} - N_{//})^2 + N_\perp^2\right]\right\} \qquad (3.3.4)$$

where: k_o is the wavenumber, $N_{//,opt}^2 = [Y/(Y+1)]$, $Y = (\omega_{ce}/\omega)$, ω_{ce} is evaluated at the cutoff and ω is the wave frequency. For fundamental EBW this B-X-O emission window is located at about 35° from the major radial direction. The emission window has a width that increases with decreasing L_n at the O-mode

cutoff, so that using a local limiter to steepen L_n should also improve coupling via O-X-B conversion. Recent modeling indicates that by controlling the ellipticity of the launched electromagnetic wave it is possible to obtain efficient (> 80%) EBW coupling efficiency as L_n at the EBW mode conversion layer varies. At this time, however, it is not clear if controlling the ellipticity of the launch wave will be sufficient by itself to allow efficient O-X-B coupling, which is resilient to changes in L_n at the O-mode cutoff. It may still be necessary to use a local limiter to steepen L_n in combination with polarization control to realize a robust O-X-B launcher design.

3.3.10 Status of EBW Mode Conversion and Coupling Experiments

Because of the fundamental properties satisfied by the mode conversion equations: linearity, energy flow conservation, and time reversibility [26,27] the emission results from CDX-U and NSTX can be used for studying mode conversion excitation of EBWs for heating and current drive in ST plasmas.

For fundamental and second harmonic EBWs CDX-U and NSTX are over-dense beyond the LCFS on the outboard side. Second harmonic EBWs from the plasma core convert to X-mode near the LCFS and fundamental EBWs mode-convert between the LCFS and the vacuum vessel wall. Mode-converted fundamental and second harmonic EBW emission from NSTX and CDX-U has been measured normal to the magnetic field with microwave radiometry. Radiometers have operated in the 8-18 GHz band on NSTX and 4-12 GHz band on CDX-U [28]. The radiometers are calibrated absolutely with a Dicke-switched blackbody calibration source. On NSTX, dual-ridged antennas have so far viewed the emission through a vacuum window and were oriented to accept, predominantly, X-mode polarized emission during the current flat top. On CDX-U, initial measurements were made with a similar arrangement, but later measurements used an in-vessel quad-ridged antenna that incorporates a local limiter.

The radial localization of the EBW emission source was confirmed on CDX-U by perturbing the T_e profile with a series of cold gas puffs, a technique used earlier by Laqua *et al.* [25]. The cold gas puffs locally cooled the plasma edge, producing an inward propagating temperature response. The delay in the

arrival time of the temperature pulse was found to be a maximum for EBWs emitted from the Shafranov-shifted magnetic axis at $R = 40$ cm [29]. This verification that the EBW emission source is localized at the ECE resonance is an independent confirmation of the localization of the measured emission and justifies a comparison between the measured EBW T_{rad} and Thomson scattering T_e profiles.

The natural steepening of the edge-density gradient that occurs at the L to H transition can enhance the conversion and tunneling efficiency of both the B-X and B-X-O conversion processes if the steepening occurs in the vicinity of the EBW mode-conversion layer. This has been observed for B-X-O conversion on MAST [30] and B-X conversion on NSTX [31]. In NSTX plasmas with H-mode transitions, the mode-converted EBW emission is observed to increase by up to a factor of three at L to H transitions. The emission increase is coincident with steepening of the edge-density profile during the H-mode. L_n data from Thomson scattering were used to calculate C. Good agreement was found between the measured EBW T_{rad}/T_e and the calculated C using the measured L_n [32]. However, even during the H-mode phase the B-X conversion efficiency on NSTX is only 10-15%. Similarly, on CDX-U T_{rad}/T_e has been typically $\leq 20\%$.

Recently, experiments on NSTX have used the HHFW antenna structure as a local limiter to steepen L_n in the B-X conversion region and hence improve the B-X conversion efficiency. An EBW radiometer and a microwave reflectometer that measured the density profile in the scrape-off were co-located near the midplane between two of the HHFW antenna straps. When the gap between the plasma edge and the HHFW antenna was reduced from a few centimeters to close to zero, L_n shortened from ~ 2.0 cm to ~ 0.7 cm and the EBW T_{rad}/T_e increased from 10% to 50%, in good agreement with theoretical predictions using the measured L_n [33]. Rather than relying on the L_n that occurs naturally, a local adjustable limiter can control and optimize L_n for maximum C. An in-vacuum antenna/Langmuir probe assembly that can scan in major radius was installed on CDX-U [34]. In order to vary L_n for maximum mode conversion efficiency the antenna/probe assembly was surrounded by a limiter that could be positioned at different major radii relative to the antenna. Four Langmuir probes continuously measured the density profile in front of the antenna. The antenna used on CDX-U was a quad-ridged, broadband horn that could simultaneously measure O-mode and X-mode polarized emission. Data from the antenna/probe assembly showed that L_n at the fundamental B-X conversion layer could be shortened from 3-6 cm to about 0.7 cm when the limiter was inserted in front of the antenna (Fig. 3.3.9). As a result, the B-X conversion

efficiency, inferred from the EBW T_{rad}/T_e ratio, was increased by an order of magnitude. The mode-converted EBW emission on CDX-U was observed to fluctuate rapidly (~ 10 kHz) and was anti-correlated with the electron density fluctuation at the Langmuir probe closest to the B-X conversion layer. High time resolution (~1 μs) electron density data, obtained simultaneously from the Langmuir probes, has allowed measurement of L_n fluctuations and the calculation of the fluctuations in C. While there was correlation between fluctuations in C and the EBW T_{rad}, there were clearly EBW T_{rad} fluctuations that did not correlate. Refractive effects corresponding to MHD activity probably contributed about half of the EBW T_{rad} fluctuations in CDX-U, but this effect should be less serious on NSTX since the plasma is considerably larger.

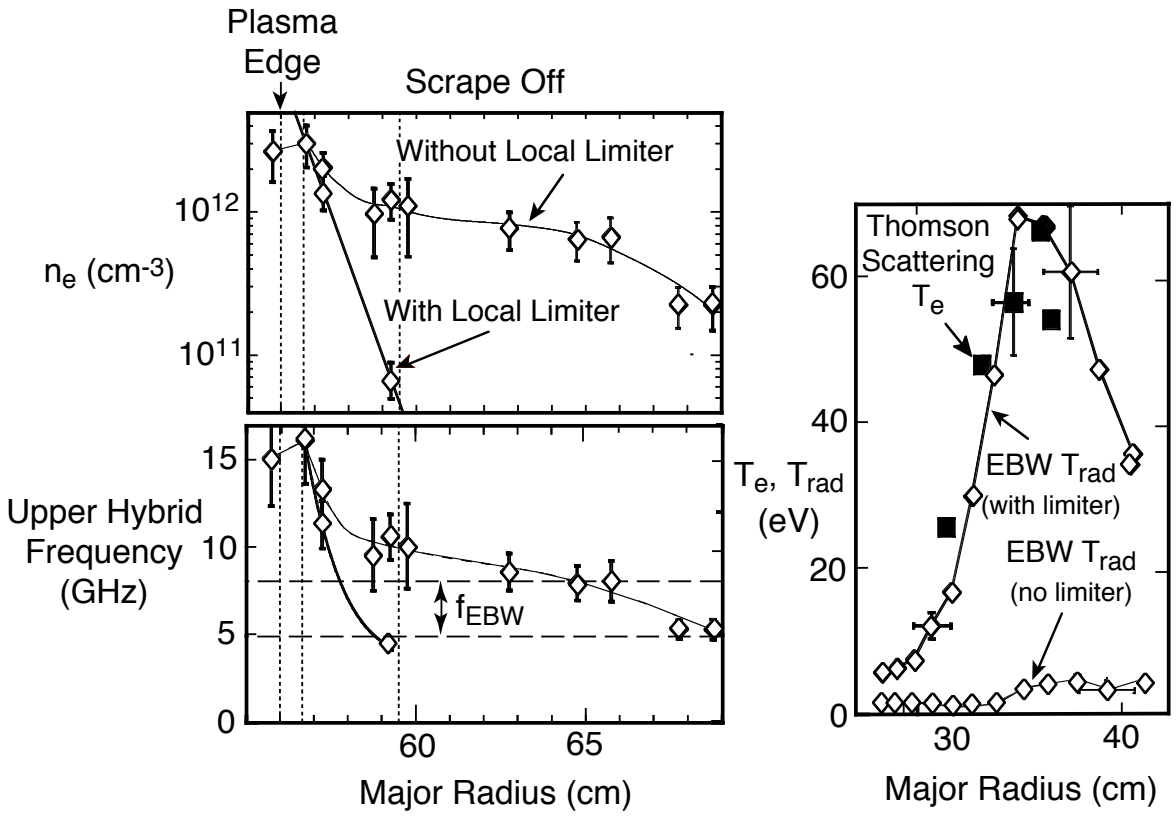

Figure 3.3.9 L_n = 3-6cm without a local limiter (thin line and diamonds) was reduced to ~0.7cm with the local limiter inserted close to the LCFS (thick line and diamonds). UHR frequencies calculated for the scrape density profiles above. The frequency range of fundamental EBW emission is indicated. The figure on the right shows that with local limiter EBW T_{rad} ~ Thomson scattering T_e.

For the 2004 NSTX experimental campaign, a pair of quad-ridged horn antennas with radially adjustable carbon limiters has been installed in NSTX in order to replicate the high B-X mode conversion results obtained on CDX-U. A frequency swept O-mode reflectometer is being integrated into the antenna assembly in order to simultaneously measure the local L_n behavior at the UHR. Also, a modification has been made to the radiometer view in the HHFW antenna used previously to measure B-X conversion so that it now views obliquely to measure B-X-O emission. The NSTX EBW emission experiments in 2004 are being performed to establish whether mode conversion efficiencies > 80% can be reliably achieved on NSTX.

Experiments to study EBW heating via mode conversion on MAST with over one megawatt of 60 GHz RF power during 2003 can also provide data that validates the use of mode-converted EBW to heat electrons and drive current locally in ST plasmas. NSTX physicists will be collaborating with the MAST research staff during these EBW experiments. Also, EBW heating experiments with about 100kW of RF power will begin on MST at the University of Wisconsin in 2003. It should be noted that recently EBWCD has been successfully demonstrated on the W-7AS stellarator [35]. The magnitude and localization of the EBW-driven current on W7-AS agreed wel1 with theoretical predictions and notably the normalized current drive efficiency compared favorably with normalized ECCD current drive efficiencies obtained previously on stellarators and low aspect ratio tokamaks.

3.3.11 Status of EBW Heating and Current Drive Modeling

The EBW MC emission studies on CDX-U and NSTX also validate the MC physics for EBWH and EBWCD [26]. EBWH and EBWCD can optimize the magnetic equilibrium and suppress deleterious MHD in ST plasmas that might otherwise prevent access to high operation by locally driving currents directly via EBWCD or indirectly with EBWH using the bootstrap effect. Deposition out to r/a ~ 0.8 may be required for MHD suppression in NSTX. Placing the EBW launcher well above or below the mid-plane on the low-field side has several benefits; large uni-directional $n_{//}$ shifts needed for efficient CD can result even with an $n_{//} \sim 0$ launch [36] and the launcher can be located where there is generally less competition for vacuum vessel access. Interestingly, EBWCD modeling for NSTX equilibria indicates

that the large trapping region in a ST plasma can result in the EBWCD being overwhelmingly dominated by Okhawa current drive at r/a > 0.3, rather than Fisch-Boozer current drive. As a result the current drive efficiency increases with r/a.

Figure 3.3.10(a) shows a GENRAY [37] calculation for a bundle of 15 GHz EBW rays launched from 65 degrees above the mid-plane of a β ~ 30% NSTX plasma. The launched rays in this example have a range of $n_{//}$ between 0.5 and 0.7. Figure 3.3.10(b) shows the significant $n_{//}$ upshift that occurs during the first 10 cm the rays travel into the plasma. 95% of the EBW power is deposited at the second harmonic electron cyclotron resonance within 7-13 cm from the plasma edge, shown by the grey shaded region in Fig. 3.3.10(a) and Fig. 3.3.10(b).

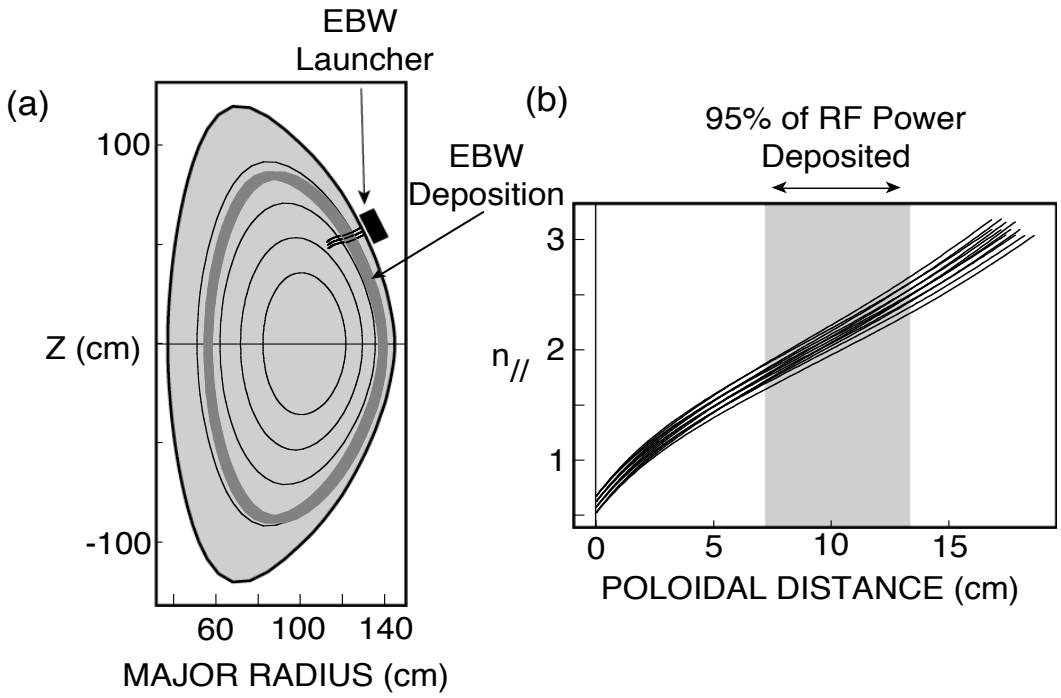

Figure 3.3.10 (a) GENRAY ray tracing calculation for 15 GHz EBWs launched from a location at a poloidal angle 85 degrees above the mid-plane of a NSTX β ~ 30% fully non-inductive plasma equilibrium. 12 rays are launched with $n_{//}$ from 0.5 to 0.7. EBW rays are projected on to a poloidal cross-section. (b) Plot of $n_{//}$ versus poloidal projected distance along the ray show a significant shift in $n_{//}$ within 5-10 cm of the plasma edge.

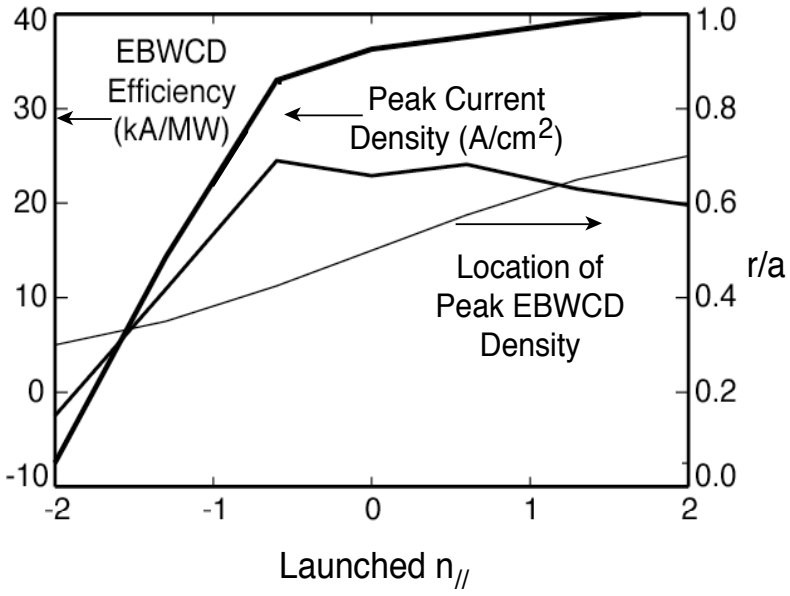

Fig. 3.3.11 EBWCD efficiency, peak driven current density and location of the peak driven current versus launched $n_{//}$, for 1 MW of 15 GHz EBW power launched 65 degrees above midplane into a β ~ 30% NSTX plasma.

Changing the launch $n_{//}$ allows some control over the radial location of the EBW deposition location without changing the launch frequency or toroidal field. Modeling of the EBWCD was performed with the CQL3D bounce-averaged Fokker-Planck code [13] for a range of launch $n_{//}$ values between –2 and +2 and the results are shown in Fig. 3.3.11. The Peak of the EBWCD was varied from r/a = 0.4 to r/a = 0.7 by increasing the launched $n_{//}$ from –0.5 to 2, with very little change in peak driven current density and a small increase in CD efficiency from 35 to 40 kA/MW. For this equilibrium, the q=1.5 and q=2 surfaces where NTMs may grow are located at r/a = 0.3 and 0.5, respectively. Some variation of poloidal launch angle may allow efficient current drive at smaller r/a, and is being studied. The dimensionless current drive efficiency, ζ_{ec}, is about 0.4 [38], with launch $n_{//} \sim 0$. This is comparable to the ζ_{ec} obtained for ECCD in DIII-D [39]. The positive current values are due to Okhawa current drive where passing electrons are driven to higher perpendicular velocities into the trapped region of phase space. The most negative launched values of $n_{//}$ result from the penetration of the EBWs to higher aspect ratio where Fisch-Boozer current drive dominates and drives current in the opposite direction.

In addition to neoclassical tearing mode stabilization, integrated scenario development of a fully non-inductive, β ~ 40% NSTX plasma will benefit from the flexibility of off-axis current drive at the level of 100 kA or above (Chapter 4). Modeling indicates that at least 100 kA of off-axis current drive between r/a = 0.4 and 0.8. EBWCD can potentially be driven off-axis if ~ 3 MW of EBW power is delivered to the

plasma. During 2003, a scoping study to explore the sensitivity of the EBW current drive efficiency to RF launch parameters (e.g., poloidal launch angle, $n_{//}$ and frequency) will continue with the GENRAY ray tracing code and the CQL3D Fokker-Planck code. This scoping study will include developing scenarios for EBW-assisted non-inductive plasma startup. The GENRAY EBW ray tracing code presently requires rays to be launched as EBWs inside the plasma; in future the EBW modeling will include both a realistic antenna pattern and refraction at the mode conversion layer (e.g., using the GLOSI code in collaboration with ORNL or cold-plasma admittance matrix modeling). Theoretical studies of the modification of EBW propagation, deposition and current drive efficiency by transport and bootstrap current will also be conducted in 2004-5. High RF power densities could potentially drive parametric instabilities near the mode conversion layer located near the edge of the plasma, so this will also be investigated theoretically. Other studies in collaboration with MIT will model non-thermal EBW emission and determine whether relativistic effects should be included in the propagation and damping of the EBWs.

3.3.12 Status of EBW Launcher and RF Source Technology

An EBW launcher design is being developed that will allow control of $n_{//}$ and the polarization of the electromagnetic launch wave for optimum coupling to the EBW. A steerable mirror launcher combined with a rotatable reflective grating polarizer is being considered, since it provides the greatest flexibility for optimizing EBW coupling and control of the EBW power deposition. An array of such launchers is being tested on MAST in 2003-4. Results from the MAST experience may help guide the launcher design.

The launch frequency that provides the widest radial access to NSTX, which typically operates at 0.35 to 0.45 T, is ~ 15 GHz with deposition of the fundamental electron cyclotron resonance. Presently, no high power, long pulse or continuous RF sources are available in this frequency range. Rick Temkin at MIT has proposed the development of 1 MW 15 GHz gyrotron tube. An EBW system using four of these tubes is being considered for installation on NSTX in 2006-8. This tube would operate at up to 47% efficiency, without a depressed collector. The tube would be engineered and fabricated by CPI, a company that already sells a 0.5 MW, 8 GHz tube. Thales, a European manufacturer that sells a 1.1 MW, 8 GHz gyrotron, would probably also bid to develop their own ~ 1 MW, 15 GHz tube. Since the estimated

design and development time for this tube is 18-24 months, a request for a cost and schedule quotation for developing the tube needs to be sent out during 2003. The tube development needs to begin in 2004 if it is to be used for megawatt-level experiments beginning in 2006. A TFTR neutral beam power supply that can provide power for these tubes is available, but a modular solid-state regulator will also need to be procured.

3.3.13 EBW Research Plan for 2003 - 2008

The NSTX EBW research plan for 2003-8 is predicated on providing at least 1 MW of EBW power for NSTX experiments starting in late 2006 with available power increasing to ~ 3 MW in 2008.

2003:

During this period a request for quote for the megawatt-level, ~ 15 GHz tube will be issued. A preliminary scoping study for NSTX, including EBW startup, with the GENRAY and CQL3D computer models, will be completed. The importance of relativistic effects in EBW propagation and damping, and an estimate of edge parametric effects on coupling at high powers, will be evaluated. A conceptual EBW launcher design will be developed. PPPL will collaborate with MAST researchers on initial EBW experiments at ~ 1 MW.

2004-5:

During this time, experiments will be conducted on NSTX to obtain conversion efficiencies of ≥ 80% for B-X and/or B-X-O emission. Collaboration with MAST on their EBW heating experiments will continue during this time. This work supports the IPPA milestone 3.2.1.3 to heat high □, over-dense plasmas. The design of the NSTX 3 MW heating and current drive system will be completed. The prototype mega-level ~15 GHz gyrotron will be designed and fabricated. Radial transport effects will be included in the CQL3D EBW current-drive modeling.

2006:

During this time, installation of the first ~ 15 GHz gyrotron on NSTX will be completed. Initial experiments in late 2006 will study on-axis EBW heating and spatial control of the EBW deposition. This work supports the IPPA milestone 3.2.1.3 to heat high □, over-dense plasmas.

2007-8:

During this time, the available EBW power will be increased to 3 MW. EBW plasma current generation and control will be investigated. Plasma current startup studies with EBW alone and in conjunction with CHI will be started. This work supports the IPPA milestone 3.2.1.4. Studies of NTM suppression with EBWCD will begin. At least 100 kA of off-axis EBWCD will be available to stabilize high-beta fully non-inductive plasmas in 2008. This work supports the IPPA milestone 3.2.1.2, the suppression of high □-limiting MHD.

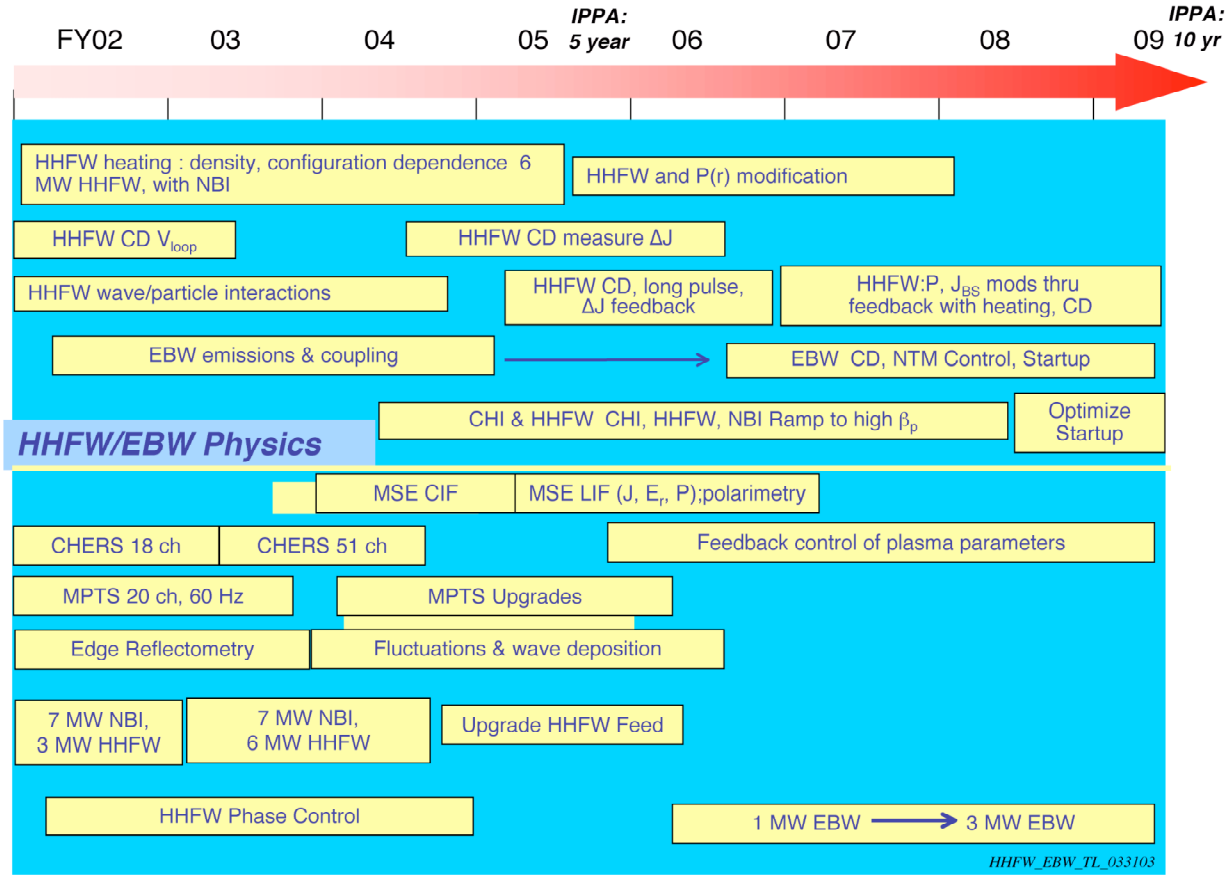

References

[1] Ono, M., et al., Physics of Plasmas, **2**, 4075 (1995).

[2] Lashmore-Davies, C.N., et al., Physics of Plasmas **5**, 2284 (1998).

[3] Ryan P.M., et al., Fusion Engineering and Design **56-57**, 569 (2001).

[4] Wilson, J.R. et al., submitted to Physics of Plasmas

[5] Brambilla, M., Plasma Physics and Controlled Fusion, **41**, 1 (1999); Brambilla, M. Plasma Phys. Control. Fusion **44**, 2423 (2002).

[6] Mau, T.K., et al., *Radio Frequency Power in Plasmas* (Proc. 14th Topical Conf. Oxnard CA, 2001) American Inst. of Physics, New York (2001) 170.

[7] Smithe, D.N., et al., in *Radio Frequency Power in Plasmas*, (AIP, NY, 1997) p.367

[8] Jaeger, E.F., et al., Phys. Plasmas **8**, 1573 (2001).

[9] Menard, J., Majeski, R., Kaita, R., Ono, M., Munsat, T., Phys. Plasmas **6,** 2002 (1999).

[10] Smithe, D.N., et al., Nuclear Fusion **27**, 1319 (1987).

[11] Ryan, P.M., Rosenberg, A.L., Swain, D.W., Wilson, J.R., Batchelor, D.B., *et al*., "ICRF Heating and Current Drive on NSTX with High Harmonic Fast Waves", in *19th International Conf. on Plasma Physics and Controlled Nuclear Fusion Research*, paper IAEA-CN-94/EX/P2-13, Lyon, France (2002).

[12] Dumont, R.J., Phillips, C.K. and Smithe, D.N., "ICRF wave propagation and absorption in plasmas with non-thermal populations", in Controlled Fusion and Plasma Physics, 26B, paper P-5.051 (29th EPS Conference, Montreux, Jun. 17-21, 2002); also Dumont, R.J., Phillips, C.K. and Smithe, D.N, "Effects of non-Maxwellian species on ICRF Wave Propagation and Absorption in Toroidal Magnetic Confinement Systems", to be published in Proceedings of the 15th Topical Conference on Radio Frequency Power in Plasmas, Grand Teton National Park, May 19-22, 2003.

[13] Harvey, R.W., et al., Proc. IAEA Tech. Com. on Advances in Simulation and Modeling of Thermonuclear Plasmas, Montreal (IAEA, Vienna, 1993) p. 489.

[14] Ehst, D. and Karney, C.F.F., Nuclear Fusion **31**, 1933 (1991).

[15] http://aida.physics.wisc.edu/~jwright/

[16] Nakajima, S., and Abe, H., Phys. Rev. A **38**, 4373 (1988).

[17] Sugai, H., Phys. Rev. Lett. **47**, 1899 (1981).

[18] Ram, A.K., and Schultz, S. D., Phys. of Plasmas **7**, 4084 (2000).

[19] Preinhaelter, J. and Kopécky, V., Plasma Phys. **10**, 1 (1973).

[20] Weitzner, H. and Batchelor, D.B., Phys. Fluids **22**, 1355 (1979).

[21] Mjølhus, E. J., Plasma Phys. **31**, 7 (1984).

[22] Nakajima, S., and Abe, H., Phys. Lett. A **124**, 295 (1987).

[23] Hansen, F.R., et al., Plasma Phys. **39**, 319 (1988).

[24] Laqua, H.P., et al., Phys. Rev. Lett. **78**, 3467 (1997).

[25] Laqua, H.P., et al., Phys. Rev. Lett. **81**, 2060 (1998).

[26] Ram, A.K., et al., Phys. Plasmas **9**, 409 (2002).

[27] Bers, A. and Ram, A.K., Phys. Lett. A **301**, 442 (2002).

[28] Taylor, G., et al., Rev. Sci. Instrum. **72**, 285 (2001).

[29] Munsat, T., et al., Phys. Plasmas **9**, 480 (2002).

[30] Akers, R.J., et al., Phys. Rev. Lett. **88**, 035002 (2002).

[31] Maingi, R., et al., Phys. Rev. Lett. **88**, 035003 (2002).

[32] Taylor, G., et al., Phys. Plasmas **9**, 167 (2002).

[33] Taylor, G., et al., Phys. Plasmas **10**, 1395 (2003).

[34] Jones, B., et al. Phys. Rev. Lett. **90**, 165001 (2003).

[35] Laqua, H.P., et al., Phys. Rev. Lett. **90**, 075003 (2003)

[36] Forest, C.B. et al., Phys. Plasmas **7**, 1352 (2000).

[37] Smirnov, A.P., and Harvey, R.W., Bull. Am. Phys. Soc. **40**, 1837 (1995).

[38] Luce, T.C., et al., Phys. Rev. Lett., **83**, 4550-4553 (1999).

[39] Petty, C.C., *et al*., "Electron Cyclotron Wave Experiments on DIII-D", *Proc. 14th Topical Conference on Radio Frequency Power in Plasmas*, edited by T.K. Mau and J. deGrassie, AIP Conf. Proc. 595, Melville, New York, 2001, pp. 275-281.